Image Cover Sheet

CLASSIFICATION	SYSTEM NUMBER
UNCLASSIFIED	149000

TITLE

CHARACTERIZATION AND CALIBRATION OF A PULSED LASER SYSTEM FOR SINGLE EVENT UPSET SIMULATION

System Number:

Patron Number:

Requester:

Notes:

DSIS Use only:

Deliver to: FF

National Defence / Défense nationale

CHARACTERIZATION AND CALIBRATION OF A PULSED LASER SYSTEM FOR SINGLE EVENT UPSET SIMULATION

by

G.T. Pepper and A. Fechete

DEFENCE RESEARCH ESTABLISHMENT OTTAWA
REPORT N0. 1241

Canada

November 1994
Ottawa

National Défense
Defence nationale

CHARACTERIZATION AND CALIBRATION OF A PULSED LASER SYSTEM FOR SINGLE EVENT UPSET SIMULATION

by

G.T. Pepper and A. Fechete
Space Systems and Technology Section
Radar and Space Division

DEFENCE RESEARCH ESTABLISHMENT OTTAWA
REPORT NO. 1241

PCN
041LS

November 1994
Ottawa

ABSTRACT

A pulsed Nd:Glass laser facility that was developed at Defence Research Establishment Ottawa, for the simulation of single event upsets (SEUs) in electronics, is described in detail. The performance of the laser system, the associated instrumentation and data acquisition systems were extensively characterized during the process of studying the charge collected in a silicon p-i-n photodiode, due to laser and ion-induced SEU. Laser simulation of SEUs is demonstrated to be an accurate, convenient, complementary method to ion accelerator-based SEU experimentation.

RÉSUMÉ

Ce rapport décrit un système développé et utilisé au Centre de recherches pour la Défense à Ottawa, pour simuler l'effet de perturbations isolées produites par des ions sur des dispositifs électroniques. Le système est composé d'un laser à impulsion au Nd:Verre, d'un système de saisie de données et d'instruments de mesures. Les performances du système sont évaluées à partir de l'étude de la charge produite par un laser et par des ions. Dans chaque cas, la charge est captée par une photodiode P-I-N. Nous concluons que le système de simulation au laser est précis, simple et complémentaire aux essais basés sur un accélérateur d'ions.

EXECUTIVE SUMMARY

Pulsed lasers have proven extremely useful in simulating the effect known as single event upset (SEU) in semiconductor devices. In the upper atmosphere or the space environment, SEU can result from the passage of a single energetic charged particle through a semiconductor device. The consequence of this action can range from a loss of information in a digital system, to the destruction of the device. In order to study SEU effects in electronics, particle accelerators have been used traditionally. More recently, pulsed lasers have also been used for this work because of the inherent practical and technical advantages gained by their use. In this report, a pulsed laser facility developed at DREO for SEU simulation is described and characterized. Experimental results are presented which demonstrate the calibration techniques used to relate SEU data obtained with both pulsed lasers and particle accelerators.

CONTENTS

LIST OF ILLUSTRATIONS

LIST OF TABLES

1.0 INTRODUCTION

The use of pulsed lasers for the simulation of single event upsets (SEUs) in semiconductor devices has proven to be a valuable tool for both the scientific investigation of SEU phenomena and the engineering development and qualification of SEU hardened devices and circuits. The interest in and the acceptance of the use of lasers for SEU studies is evidenced by the fact that in the recent IEEE Annual Conference On Nuclear and Space Radiation Effects (1992), 4 out of a total of 92 papers presented [1-4] were related to laser SEU work.

Laser SEU simulation provides many advantages which render the technique extremely attractive as a complementary method to the more traditional use of ion accelerators for SEU studies. **Laser SEU simulation is a non-destructive test procedure, producing neither total dose nor displacement** damage effects. The method is convenient, less time consuming and far less expensive than the use of an accelerator facility. Lasers can easily provide spatial SEU analysis over the surface of the die of a semiconductor device with micron resolution. Ion microbeam facilities can also attain this resolution, but the scarcity and cost of these specialized facilities inhibit their use on a wide scale. One major advantage in the use of lasers for SEU studies, which is extremely difficult to perform with an ion microbeam facility, is that laser SEU generation can simultaneously be localized both spatially and temporally. This is extremely useful when memory devices are SEU tested; the laser firing can be synchronized with respect to a system clock, making it easy to probe a device during the entire memory read/write access cycle, during which the SEU sensitivity at a given node or location may vary.

With all physical simulation techniques, the data obtained via simulation must be quantitatively related to

the actual physical phenomena and parameters of interest. With laser-induced SEU, the charge deposition (i.e. the creation of electron-hole pairs) by a single energetic ion in a semiconductor device is simulated by focusing a short pulse of appropriate wavelength optical radiation onto the surface of a semiconductor die. The laser radiation that penetrates the semiconductor material is absorbed to some extent and can result in electron-hole pairs being liberated within a very localized volume, similar to that produced by the passage of an energetic ion. Laser parameters such as the wavelength, pulse-width and the diameter of the focused laser beam on the semiconductor surface must be judiciously selected so as to reproduce the temporal and spatial charge distributions that the passage of an ion would generate within the semiconductor device. These issues have been addressed at length elsewhere (for example, see [2,5]). To permit a meaningful comparison of the SEU data obtained with energetic ions and the laser, for a given device, the relationship between ion energy (for a given ion type and charge state), or linear energy transfer (LET), versus incident laser pulse energy (for a given pulse-width and focused spot size on the semiconductor's surface) must be established.

Both digital and analog semiconductors can be susceptible to SEU. With digital devices, the typical macroscopic SEU response can range from the so-called soft error or bit-flip to latch-up and device burn-out. With analog devices, SEU can manifest itself in a multitude of ways; undesired current flow across a junction, the turn on of a CMOS FET, or even device destruction due to excessive current flow. Digital semiconductor devices, when viewed in terms of their fundamental building blocks, are essentially analog devices. They are usually constructed of many analog components such as transistors (e.g. MOSFETs), diodes, resistors etc. However, when the digital device response to SEU is studied by monitoring the externally accessible

electrical connections to the device, it is mainly digital transitions or states that are measured. From the viewpoint of understanding the physics of the ion interaction leading to SEU in a digital device, this methodology limits the useful data obtained to threshold phenomena, i.e. the point at which a soft error occurs. With analog devices the same limitation is not relevant since the analog response of the device to SEU is usually continuously variable. Measuring the SEU response of an analog device rather than a digital device affords the capability of obtaining SEU response data over a much larger dynamic range. This seldom recognized point has important ramifications, especially for the calibration of a pulsed laser SEU simulation facility.

For the purpose of SEU simulation with a pulsed laser, it is necessary to calibrate the experimental system in order to establish a correlation between the laser pulse energy and the equivalent ion energy, or ion LET, even if the correlation is device specific. From a practical viewpoint, it is necessary to establish the accuracy and repeatability of the "simulation" data obtained and to determine the dynamic range over which the ion energy or LET can be simulated. For semiconductor devices that have had ion SEU measurements performed on them, but have yet to be studied with the laser SEU technique, a calibration of a similar device provides a useful, approximate guideline as to what range of laser pulse energy is appropriate to induce the same magnitude (e.g. the amount of charge collected or the onset of a soft error) of SEU effect. This calibration data can also prove useful as a diagnostic tool to ensure the integrity of the performance of the laser and data acquisition systems.

In this paper, we discuss the pulsed Nd:Glass laser facility that was developed at Defence Research Establishment Ottawa for the simulation of SEUs in semiconductor devices. We also present the results of an

extensive calibration of our experimental system in terms of laser pulse energy versus ion energy and ion LET. This calibration was accomplished via the comparison of the charge collected in a Motorola MRD500 silicon pin photodiode after exposure to 1060 nm pulsed laser radiation and exposure to alpha particles of 5.48 MeV maximum energy. The MRD500 pin diode was selected for this study, as opposed to a digital device, due to the reasons discussed in the preceding two paragraphs.

2.0 EXPERIMENTAL SYSTEMS

The MRD500 silicon p-i-n photodiode used in this work, manufactured by Motorola Incorporated, was selected because of its fast response time (t_{rise}<1 ns), optical sensitivity, low cost and availability of device structural and compositional data. The MRD500 die measures 30 mils x 30 mils with an active area of 380 square mils [6]. For both the laser and alpha particle irradiation experiments, the convex glass lens and part of the TO-18 package were removed from the device to fully expose the MRD500 die.

For an accurate comparison between the charge collected in the MRD500 diode due to irradiation with alpha particles and pulsed optical radiation from the laser, the same de-capped diode and charge measurement apparatus were used for both series of experiments. For charge collection measurements, the MRD500 diode was reverse-biassed at 50 volts, which ensured that the device was operated in the fully depleted mode[6].

The charge collection measurement electronics consisted of an Ortec model 142IH charge sensitive preamplifier, an Ortec model 571 amplifier and an ORTEC ACE, 4096 (4K) channel multi-channel analyzer (MCA). The pulse-height measured by the MCA is linear with respect to the charge

collected from the MRD500 diode by the preamplifier. The conversion gain of the preamplifier is approximately 45 mV/MeV (Si equivalent) [7]]. The pulse-shaping time constant selected for the model 571 amplifier was 2 microseconds, which is a typical value for use in alpha particle spectroscopy with surface barrier detectors.

One of the main experimental concerns in this work was the reproducibility of pulse height data obtained with our charge measurement apparatus. The charge collection electronics had to be moved between two different areas of the laboratory for the ion and laser pulse height measurements, which necessitated cycling the a.c. power to the equipment. An ORTEC model 480 pulser was used to inject a reference signal into the preamplifier's test input to monitor and correct for changes in system gain and d.c. offsets due to power cycling and long term drifts. The amplitude was selected via a combination of four front panel switches on the pulser. Three sets of switch settings were pre-determined to yield three Gaussian-shaped reference peaks - at the low, middle and high channel regions of the ADC. The centroid channels of the Gaussian distributions could then be determined from the pulse-height data. A uniform shift in the channel location of the centroid for each of the three distributions indicated a shift in the d.c. offset, while changes in gain were reflected by a change in the relative separation of the centroids. Using this data, corrections could be applied to the pulse height data obtained with the MRD500 diode. Corrections that were applied to the experimental pulse height data were small, typically less than one percent, for both gain and offset corrections. This technique also provided a cross-check on the alpha particle energy calibration discussed in the next section.

2.1 ION MEASUREMENTS

Irradiation of the MRD500 diode with alpha particles was conducted in a vacuum chamber, using a 5.55 kBq ^{241}Am alpha calibration source from Amersham Canada Limited. The non-encapsulated alpha source consisted of ^{241}Am electro-deposited in a very thin layer on a stainless steel disc of 25 mm diameter. The diameter of the active area is approximately 7 mm. The alpha source to MRD500 die geometry was arranged such that the alpha particles were incident normally to the die surface. The source-to-die distance was fixed at 5.00±0.05 cm for all measurements. This distance yielded a rate of approximately 4.33×10^{-2} alpha particles per second incident on the die's active surface (2.45×10^{-3} cm^2), in the highest vacuum (i.e. <0.02 mm Hg) attainable with our system. The rate of alpha particles incident on the MRD500 die was found to decrease with increasing air pressure in the vacuum chamber. This is a result of an increase in scattering of the alpha particles by the air molecules, as the density of air molecules increases.

^{241}Am has a half-life of 432.0 years and emits alpha particles of energy 5.48 MeV (86% relative intensity), 5.443 MeV (12.7% rel. intens.) and 5.389 MeV (1.3% rel. intens.) [8]. This source is normally considered monoenergetic as the various alpha energies are normally not resolvable with typical silicon surface barrier detectors. For the purpose of this work, all calculations and TRIM [9] Monte Carlo alpha particle transport simulations are based upon a principal alpha energy of 5.48 MeV. The manufacturer of the alpha source certifies that the energy distribution of the principal alpha emission is less than 20 keV, full-width at half-maximum, due to sample self-absorption.

The absolute air pressure in the vacuum chamber was measured using two different instruments. To measure

absolute partial air pressures in the range of 0-200 mm Hg, a Far West Technology gas fill system vacuum gauge with 0.2 mm resolution was used. For the range of 200 mm Hg to atmospheric air pressure, a mercury U-tube aneroid barometer was used, which was capable of 0.5 mm resolution.

A series of TRIM Monte Carlo simulations were performed to determine the air pressure required to obtain the desired energy of alpha particles (in the range of 0 to 5.48 MeV) incident on the MRD500 die. For a source-detector distance of 5.0 cm and using an alpha particle initial energy of 5.48 MeV, the transmitted ion energy distributions were simulated using the TRIM computer code, on a personal computer. Figure 1 shows typical TRIM simulation results for air pressures of 56.3 cm Hg, 37.5 cm Hg and 8.36 cm Hg which yielded average incident alpha energies of 0.98±0.08 MeV, 3.00±0.05 MeV and 5.00±0.01 MeV, respectively, at 20°C. The transmitted ion energy distributions are Gaussian and as expected, the FWHM of the energy distribution increases as the absolute air pressure increases. Figure 2 illustrates the calibration curve obtained via TRIM simulations for the average transmitted alpha particle energy (i.e. the average alpha particle energy that is incident on the MRD500 die) versus absolute air pressure in the vacuum chamber.

A sensitivity analysis was conducted to investigate the effect of the error in the source-detector distance (d) and the absolute air pressure (p) in the vacuum chamber, on the transmitted alpha particle energy (E_{trans}), based upon an initial alpha particle energy (E_0) of 5.48 MeV. TRIM simulations were first performed using d=5.00 cm and the appropriate air pressure (at 20°C) necessary to achieve the desired $E_{trans}(E_0,d,p)$, i.e. without consideration for error in either d or p. To determine the effect of the error in the source-to-detector distance on E_{trans}, the TRIM simulations were repeated to determine $E_{trans}(E_0,d\pm\sigma_d,p)$,

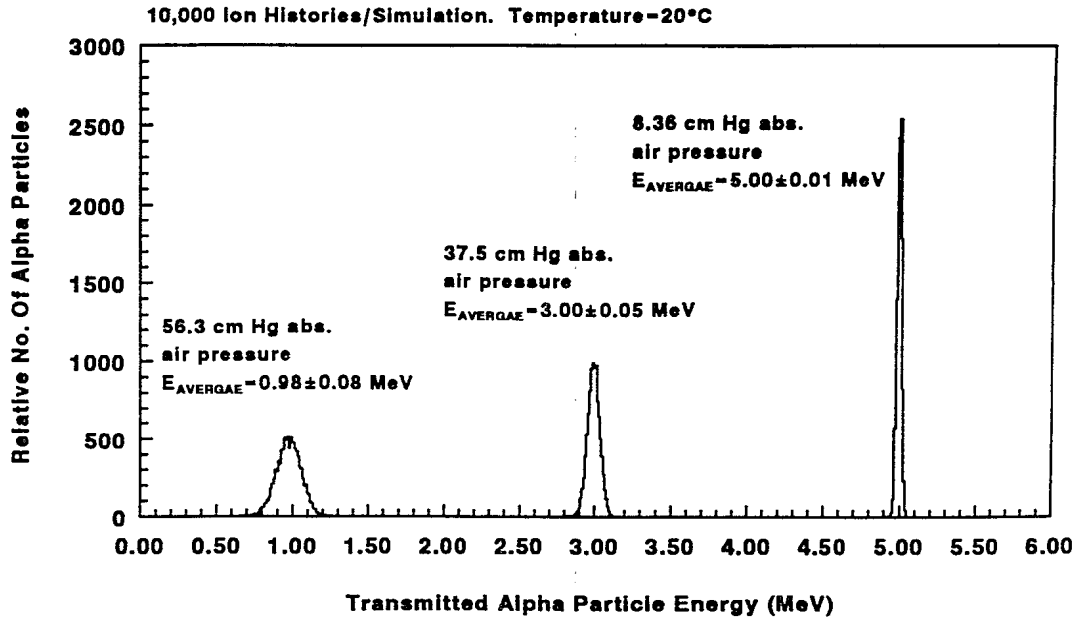

Figure 1. Typical TRIM simulation data obtained for the determination of the average transmitted alpha particle energy, for a source-detector distance of 5.00 cm and various absolute air pressures, using an initial alpha particle energy of 5.48 MeV.

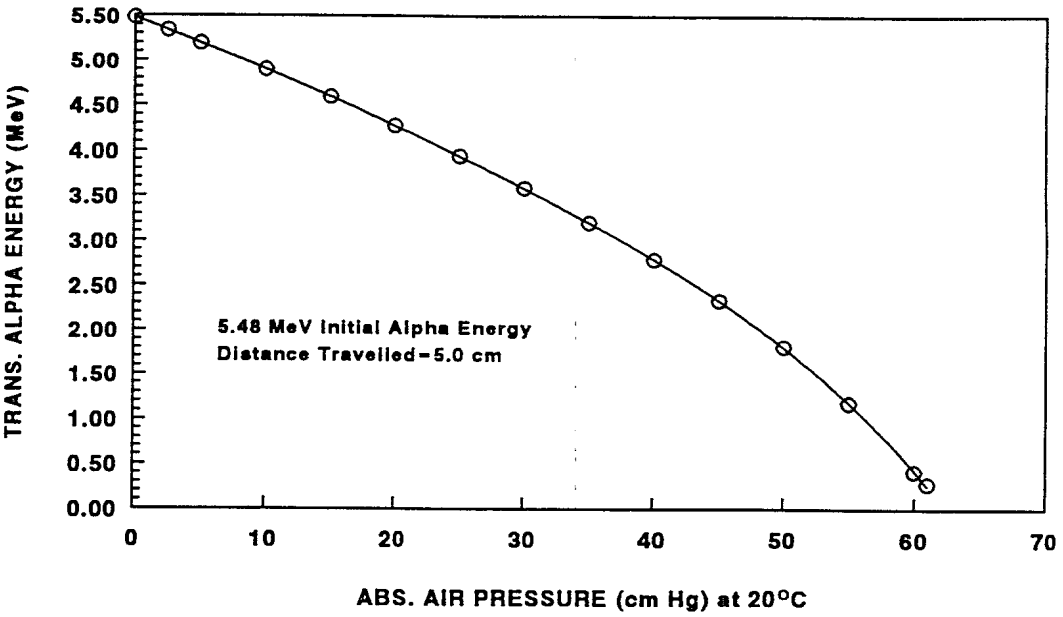

Figure 2. Summary of TRIM simulation results obtained to determine the average transmitted alpha particle energy, after traversing 5.00 cm of air, as a function of absolute air pressure, assuming an initial alpha particle energy of 5.48 MeV.

where σ_d=±0.05 cm in this work. To determine the effect of the error in the absolute pressure in the vacuum chamber on E_{trans}, TRIM simulations were performed for $E_{trans}(E_0,d,p\pm\sigma_p)$, where σ_p=0.5 cm. This value of σ_p represents a worse-case error due to long-term leakage in the vacuum chamber and not the error in the measurement of absolute pressure, which is typically less by an order of magnitude or more. The simulations were performed for $E_{trans}(E_0,d,p)\approx$3.00 MeV and $E_{trans}(E_0,d,p')\approx$1.00 MeV. The latter energy value represents a worse-case scenario, because for alpha particles in air, this energy is close to the Bragg peak energy (~700 keV from TRIM generated stopping power and range tables), which infers a maximum energy loss dE/dx. The results of the simulations are shown in Table 1. The TRIM simulation results indicate that the error in the transmitted ion energy for an expected alpha energy of 3.00 MeV is approximately 1% or less, while the error in the transmitted alpha energy for an expected alpha energy of ≈1.00 MeV might be as large as approximately 9%. This analysis demonstrates that the errors in the transmitted energy determination for our experimental arrangement were small.

Initial Alpha Energy E_0 (MeV)	Source-Detector Distance d (cm)	Abs. Air Pressure p (cm Hg)	Transmitted Alpha Energy $E_{trans}(E_0,d,p)$ (MeV)
5.48	5.00	37.51	3.00
5.48	5.05	37.51	2.97
5.48	4.95	37.51	3.03
5.48	5.00	37.51	3.00
5.48	5.00	38.01	2.97
5.48	5.00	37.01	3.03
5.48	5.00	56.32	0.98
5.48	5.05	56.32	0.89
5.48	4.95	56.32	1.06
5.48	5.00	56.32	0.98
5.48	**5.00**	**56.82**	**0.93**
5.48	5.00	55.82	1.07

Table 1. Summary of the TRIM Monte Carlo simulation analysis to determine the sensitivity of the transmitted alpha particle energy on experimental uncertainties in the measurement of the absolute air pressure (20°C) and the source-to-detector distance.

2.2 LASER MEASUREMENTS

The experimental apparatus used for the laser measurements is illustrated in figure 3. A Laser Applications, series 9300 Q-switched Nd:Glass laser was used in single-shot mode to produce approximately 1 J/pulse of 1060 nm near-infrared radiation. This type of laser is useful for SEU simulation because the 1060 nm wavelength corresponds to a photon energy of 1.17 eV, which is slightly larger than the 1.14 eV band gap of silicon at 300 K. This provides for sufficient optical penetration in silicon, while providing relatively large and near-uniform generation

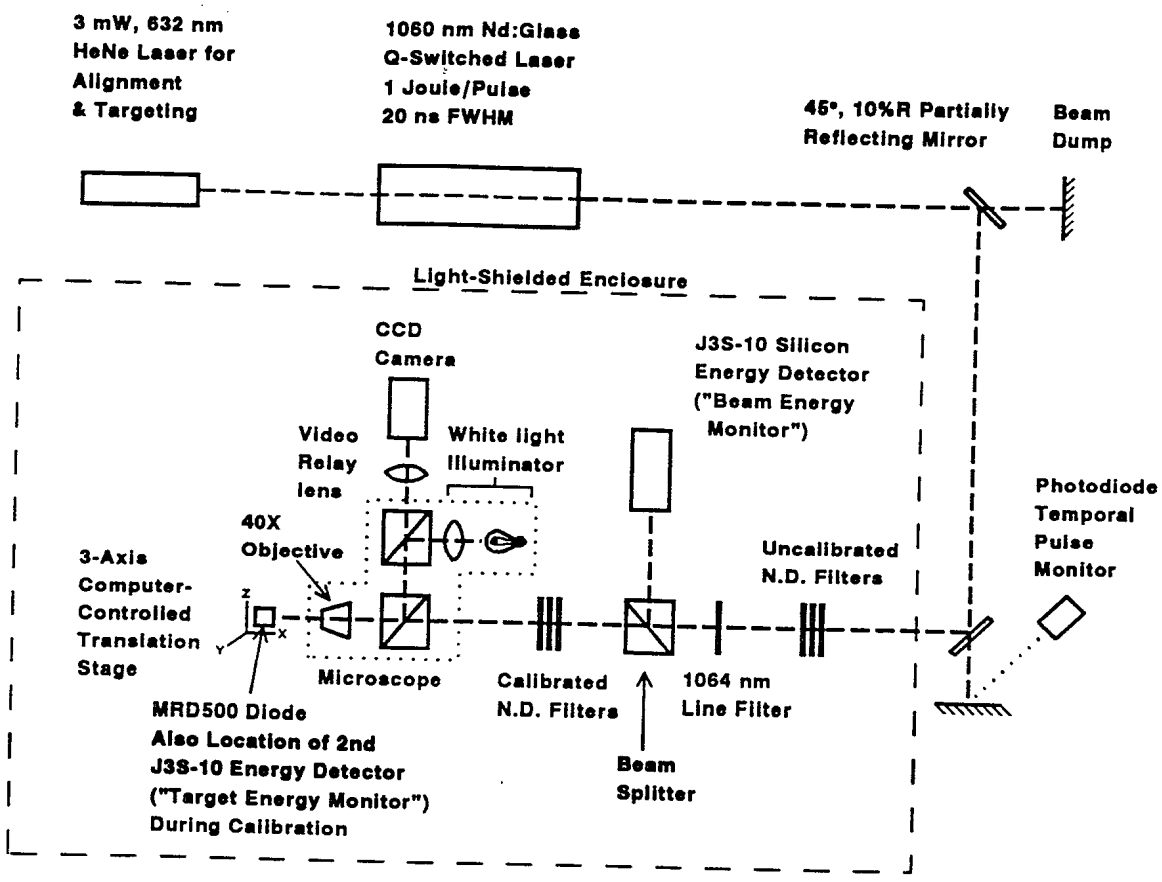

Figure 3. Experimental arrangement for laser SEU simulation.

of electron-hole pairs as a function of depth (the 1/e attenuation depth for 1060 nm photons is approximately 250 μm in Si at 300 K [2,5]).

The laser pulse-width was measured to be approximately 20 ns full-width at half-maximum (FWHM), as shown in figure 4. The exit beam diameter was approximately one-half inch (12 mm), defined by the diameter of the Nd:Glass rod and the exit aperture of the laser. The spatial beam profile, i.e. the spatial energy distribution, can best be described as approximately annular. A Gaussian (TEM_{00}) beam profile is necessary to obtain near-diffraction limited focusing performance, to achieve the smallest possible focal spot

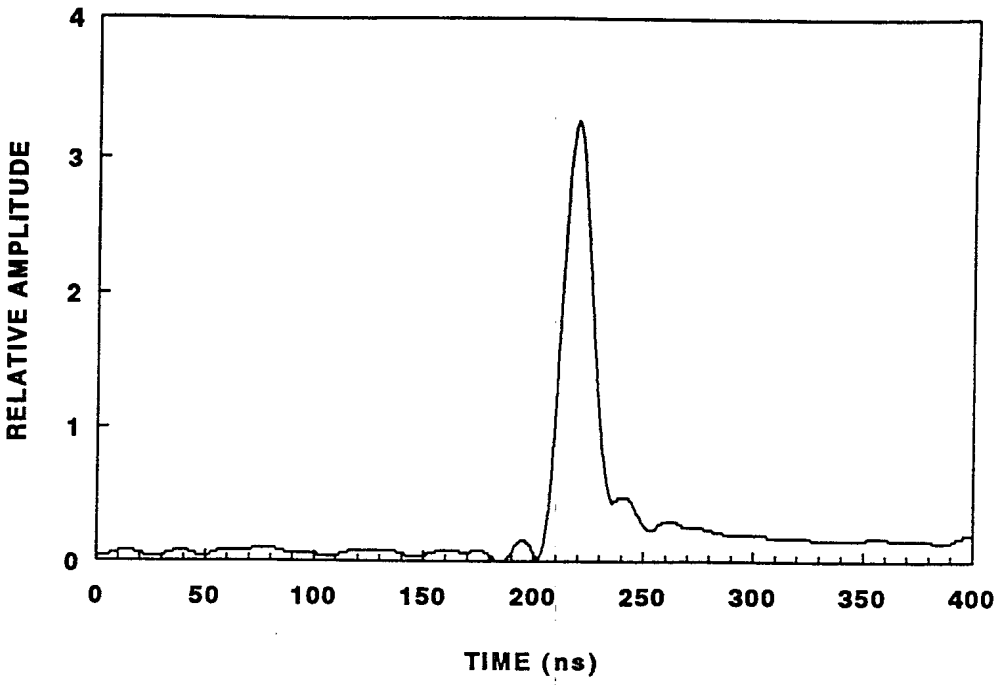

Figure 4. Temporal profile of the laser pulse, as measured by a fast photodetector. The full-width at half-maximum was 20 ns.

size when focusing the laser energy onto the surface of a semiconductor device. The most common approach to achieve a near-Gaussian intensity profile is to employ a spatial filter. Spatial filters, however, are especially difficult and time consuming to set up for pulsed infrared lasers. Alternatively, we experimented with placing various diameter circular apertures in the laser cavity to try and force the cavity oscillation mode to TEM_{00}. It was found that approximate TEM_{00} performance could be achieved with a 5/32 inch (~4 mm) diameter intra-cavity aperture. A typical two-dimensional (2-D) cross section of the beam intensity is shown in figure 5a. This 2-D intensity profile was obtained via a DREO-developed CW and pulsed-laser beam profiling instrument. The profiling instrument employs a charge-coupled device (CCD) as the detector, which consists of a one inch (3.54 cm) long, 1024 element array of photosites.

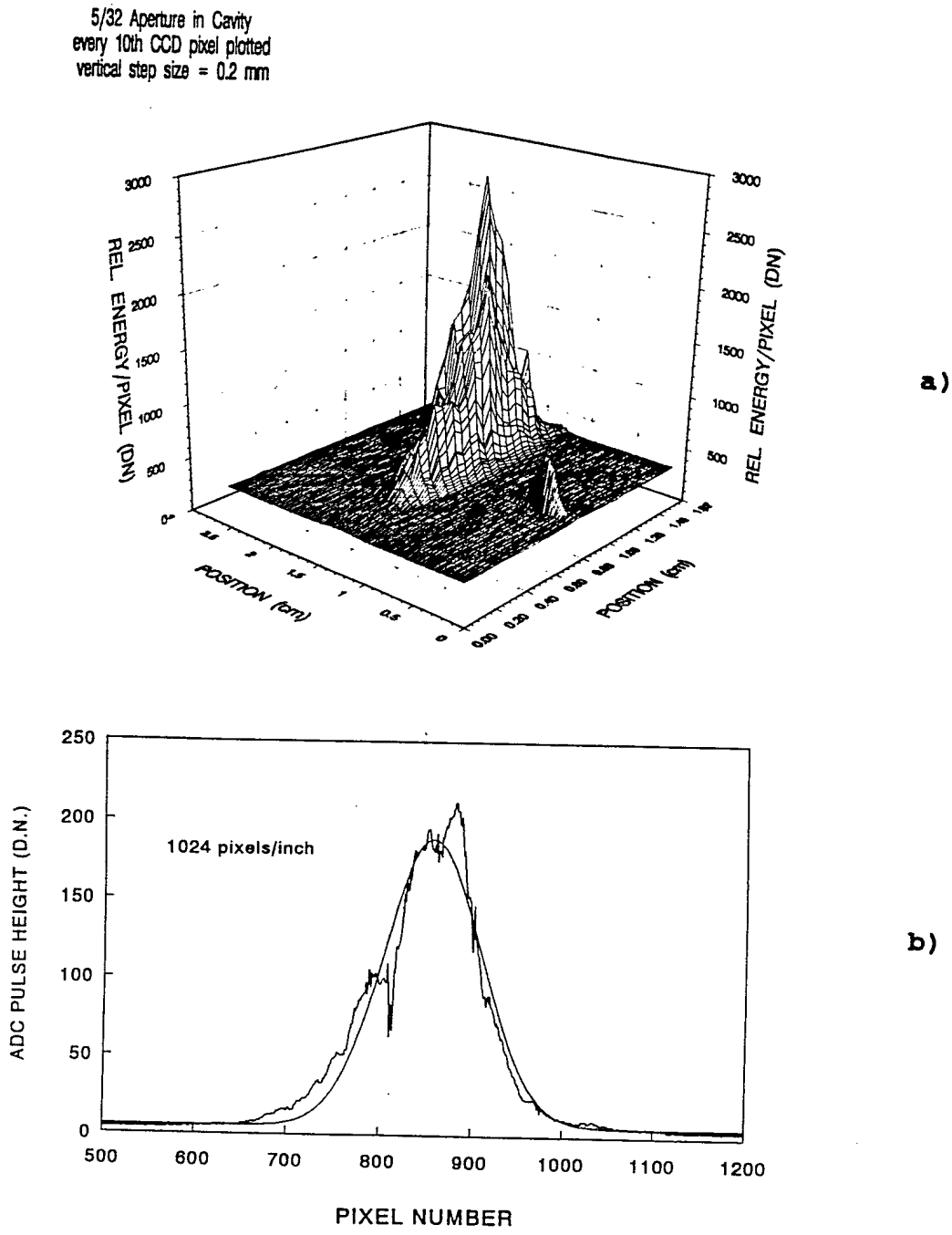

Figure 5. Measurement of the laser beam's intensity profile, performed with a DREO-developed linear CCD beam profiling instrument. A 5/32 inch aperture was used in the cavity to achieve approximate TEM_{00} performance. **a)** A 2-dimensional intensity profile and, **b)** a 1-dimensional slice through the central portion of the distribution, compared with a Gaussian distribution (smooth curve).

The CCD is attached to a 3-axis translations stage which can be stepped accurately, under computer control. The beam profiling instrument is described in detail elsewhere [10]. In figure 5a, the data was obtained by stepping the CCD vertically, in steps of 0.2 mm, while repetitively pulsing the laser. In figure 5b, a 1-D "slice" from the distribution was selected, in the vicinity of the peak. For comparison, the experimental data is shown with a Gaussian distribution (smooth curve) that was fitted to the data. The stability of the pulse energy for the system was within ±5% and the pulse width stability was approximately ±10% for the laser operating parameters selected for this work.

To perform SEU simulation using a laser, it is imperative to vary the pulse energy incident on the target semiconductor device. Usually some pulse energy control is afforded by varying an operational parameter of the laser, typically associated with the power supply. The only method available to vary the pulse energy of the 9300 series Nd:Glass laser system was via the magnitude of the pulse-forming network (PFN) voltage which was applied to the helical flashlamp when the laser was fired. It was noted in this work that the PFN voltage greatly affected the pulse-width and the pulse-width/energy stability. As the PFN voltage was reduced, the pulse energy was found to decrease, the pulse-width increased and the pulse-width/energy stability generally decreased. Although the 1 Joule per pulse energy output was much greater than what was required for our experimental work, the 4.00 kV PFN voltage selected was a compromise between the energy output and the pulse-width selection and stability. Other optical techniques, external to the laser, had to be employed to reduce the pulse energy and provide pulse energy variability.

To reduce the laser pulse energy to the nJ range required for this work, several partially reflecting (10%) mirrors were used for beam steering and several uncalibrated

neutral density filters were placed in the beam path. In addition, an optical line (i.e. thin film interference) filter with a 1064 nm centre wavelength and a 10 nm full-width at half-maximum band pass was used to render negligible the effect of optical radiation from both the flash lamp and ambient light. Both the uncalibrated neutral density filters and the line filter were located inside a light-shielded enclosure. The neutral density filters were placed before the line filter to ensure that the incident energy density was below the damage threshold of the line filter.

Also located inside the light-shielded enclosure, a beam splitter was used to direct approximately half of the pulse energy to a pulse energy monitor and the other half through a microscope system where it was focused onto the MRD500 die by a standard 40X refractive microscope objective. The pulse monitor consisted of a Molectron J3S-10 silicon Joulemeter detector, used in conjunction with a Molectron JD2000 dual channel Joulemeter Ratiometer. Coupled to the microscope was a video relay lens system and a black and white CCD camera, which permitted the viewing/positioning of the MRD500 die and the visual location of the focused laser beam "spot" on the surface of the die. The Cohu model 6510 CCD camera was used in this work. A 3-axis, computer-controlled translation stage was used for precise positioning of the MRD500 device. The resolution of the positioning system was 0.1 μm for each axis. The laser spot was focused onto the approximate centre of the MRD500 die and remained stationary for the duration of the laser SEU measurements. Spatial variation in the response of the MRD500 diode to the pulsed 1060 nm radiation, if present, was not investigated in this work.

In order to vary the energy of the pulsed 1060 nm radiation incident on the MRD500 die, it was necessary to insert various combinations of calibrated neutral density

filters in the beam path between the 50/50 beam splitter and the microscope. To calibrate energy readings obtained with the pulse energy monitor in terms of absolute energy incident on the MRD500 die, a second Molectron J3S-10 silicon Joulemeter was substituted in the place normally occupied by the MRD500 diode. The ratio of energy incident on the two energy detectors was then measured for all the filter combinations used. Thus, during later experimentation with the MRD500 diode, the 1060 nm pulse energy incident on the surface of the MRD500 die could then be accurately determined simply by applying the appropriate correction factor to the energy reading obtained with the pulse energy monitor. The fluctuation in the energy ratios obtained from the two J3S-10 detectors was determined experimentally to be less than ±2%. The J3S-10 energy detectors were calibrated by the manufacturer using a NIST traceable standard at 1064 nm wavelength. The correction factor for the response of the J3S-10 energy detectors for use at 1060 nm is negligible since the wavelength difference is so small. The accuracy of the J3S-10 energy calibration is certified by the manufacturer to be ±5% at 1064 nm. A conservative estimate of the error in the absolute energy incident on the MRD500 die is ±10% based upon considerations such as the detector calibration accuracy, the error associated with the measurement of the optical densities of the neutral density filters used in this work and our experimental method.

In order to measure the diameter (i.e. the focal spot size) of the focused 1060 nm pulsed radiation, a standard knife edge beam profiling technique was used. A straight knife edge (razor blade) was attached to the 3-axis stage and positioned at the focal point of the objective, using the CCD camera and white light illumination as a visual positioning aid. The knife edge could be scanned in either the horizontal or vertical direction perpendicular to the beam path, depending on the selection of the orientation of

the knife edge on the 3-axis stage. A J3S-10 silicon energy detector (subsequently referred to as the "target" energy monitor) was placed close to and behind the knife edge, such that the unobscured laser beam area was totally encompassed within the sensitive area of the detector (the diameter of the sensitive area of the detector is approximately 11 mm). Thus, by scanning the knife edge across the full diameter of the laser beam, while measuring the transmitted laser pulse energy with the target energy monitor, a measurement of the integral beam energy as a function of the knife edge position could be performed. In order to correct the pulse energy data taken with the target energy monitor for fluctuations in the energy output of the laser, energy readings were normalized using energy data simultaneously obtained with the pulse energy monitor. A 1 μm incremental step size was used for changing the position of the knife edge during a cross-sectional measurement of the focal spot size and an average of 5 energy readings were taken at each position.

It was expected that there might be a small difference in the focal lengths for visible and 1060 nm, near-infrared radiation, for the refractive objective. In order to ensure that we had located the optimum focus point for 1060 nm wavelength, we repeated the profiling measurements every 5 microns along the beam axis, for both shorter and longer focal lengths, relative to the visible focus position.

Figure 6 shows the result of the minimum spot size obtainable with our optics, measured using the knife edge profiling technique, for a knife edge scan that intersected the laser beam at 90° , parallel to the surface of the optics table. The focal length for 1060 nm was determined to be 50 μm less than the focal length for white light illumination. The data points shown in figure 6 represent the average of 5 consecutive readings taken at each position and the error bars reflect the standard deviation of the 5

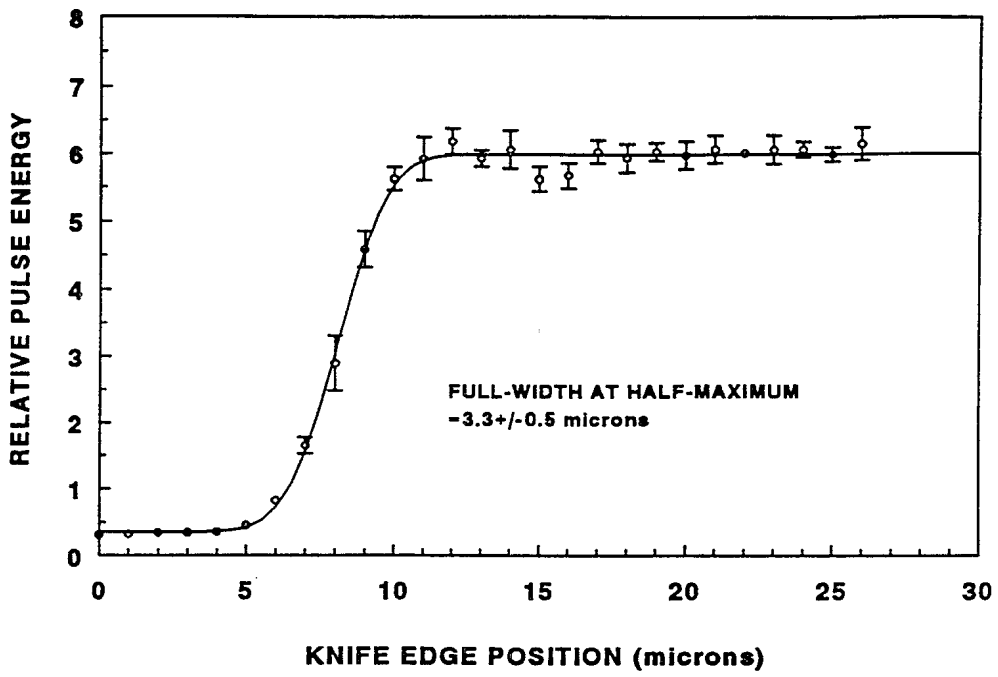

Figure 6. Measurement results for determination of the minimum spot size, for the focused 1060 nm radiation. The spot size was measured to be 3.3±0.5 μm.

values. The solid line in figure 6 represents the result of a non-linear fit of the data to an error function of the form

$$y(x) = a_0 + \frac{a_1}{2}\left[1 + \mathrm{erf}\left(\frac{x-\bar{x}}{\sqrt{2}\sigma}\right)\right] \qquad (1)$$

The spot size, defined as the FWHM of a Gaussian intensity distribution (i.e. FWHM≈2.354σ) can be determined from the parameter σ obtained from equation (1), since the error function is derived from the integral of a Gaussian distribution and in the form of equation (1), the mean ($\bar{x}$) and standard deviation (σ) of the parent Gaussian distribution are preserved. The FWHM at the focus was determined to be 3.3±0.5 μm, from the fit of the data. The

reduced chi-square (χ^2_ν) was 1.39, indicating an excellent fit. Although the data is not reproduced here, a scan in the vertical direction, i.e. 90° with respect to the horizontal scan, at the same position yielded a spot size of 3.6±0.6 μm, indicating good radial symmetry, which is expected for a TEM_{00} beam mode.

It was discovered early in the experimental work, during charge collection measurements with the MRD500 diode, that electromagnetic interference from the laser system was causing an unacceptable signal to noise ratio (SNR). The noise manifested itself during the laser pulse, for example, as relatively large, high frequency, bipolar voltage transients during the much lower frequency (and lower relative amplitude) unipolar output signal from the model 571 amplifier. During the discharge of the power supply to the flash lamp the peak current can attain values as large as 800 amperes, typically for a duration of several hundred microseconds. This pulse travels from the power supply to the laser head/flashlamp via unshielded high voltage cables several metres long, thus the potential for significant electromagnetic radiation is very great. A shielded enclosure was constructed to hold the majority of the data acquisition electronics. Good grounding techniques were employed to reduce noise coupling and ground loops. EMI/RF shielding was also provided for the MRD500 diode, mounted in a test fixture on the 3-axis translation stage. In addition, all BNC cables were doubly shielded via the use of an external braided cable shield. After these measures were implemented the SNR was greatly improved.

3.0 EXPERIMENTAL RESULTS

A typical ^{241}Am alpha energy spectrum obtained with the MRD500 diode is shown in figure 7a, for the highest vacuum attainable (<0.02 mm Hg) in the vacuum chamber. For comparison, an ^{241}Am alpha spectrum obtained with an EG&G Ortec surface barrier detector, under similar conditions, is shown in figure 7b. The energy spectrum obtained with MRD500 diode appears to have more than one peak, although the energy spectrum obtained with the surface barrier detector does not resolve the multiple alpha decay energies. Subsequent analysis of the multiple peak locations, in terms of alpha energy, discounted the possibility that two or three of the main alpha decay energies of ^{241}Am were being resolved. We can only conclude that the smaller area peak(s) below the full energy peak may have been due to non-uniformities in the energy deposition by the alpha particle and/or subsequent charge collection in the MRD500 diode. Both of these processes are likely to occur in and around the perimeter of the active (square) area of the device as the cathode metallization completely encircles it. It should be noted that surface barrier detectors are designed to ensure that the probability of "edge effects" for normally incident alpha particles (or other light ions) are virtually non-existent. This is necessary in order to maximize the energy resolution of the detector. The MRD500 was not designed to function as an alpha particle detector, but rather as an optical detector for visible and near infrared light, therefore, the deviation in performance from a surface barrier detector should not be unexpected.

From figures 7a and 7b, it was evident that the spectral line shapes in the energy spectra obtained using the MRD500 and the surface barrier detector were very similar. For the energy spectra obtained with the MRD500 diode, it was necessary to systematically determine the main peak location as a function of the absolute air pressure in

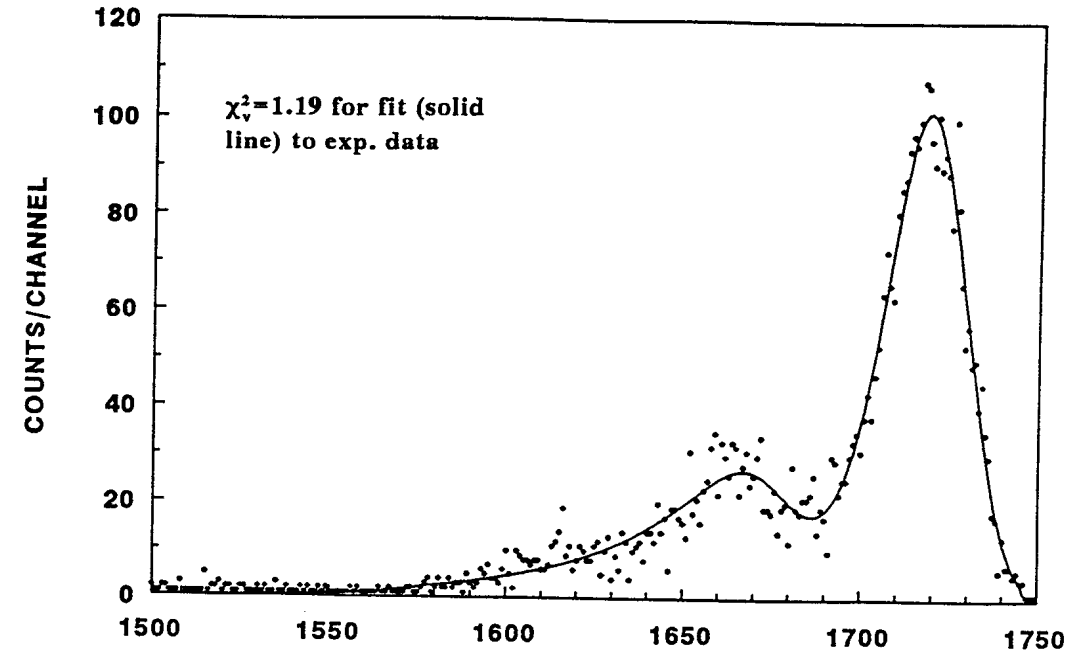

a)

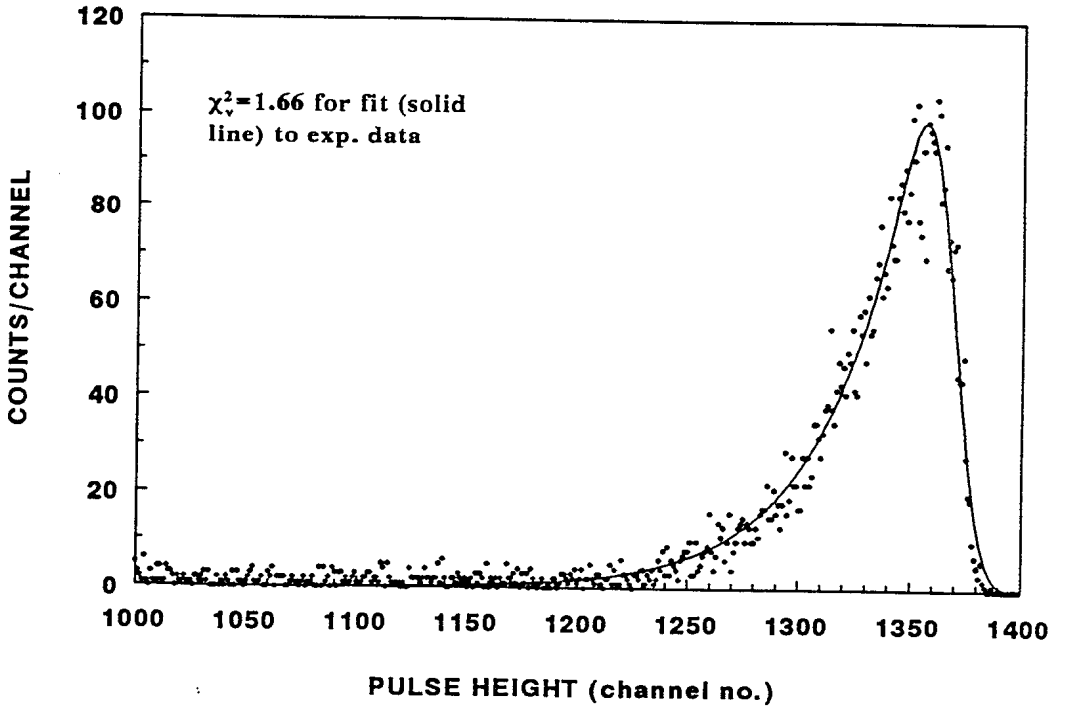

b)

Figure 7. Alpha spectra obtained with **a)** the MRD500 silicon pin photodiode and, for comparison, **b)** a surface barrier detector.

the vacuum chamber. To that end, a mathematical function was sought, via numerical experimentation on a computer, to describe the line shape. It was found that the spectral line shape could be adequately described by a mathematical function derived from the convolution of an exponential distribution (i.e. $\exp[-\beta x]$) with a Gaussian distribution, the form of which is given in the references [11, 12]. For the surface barrier detector spectrum, a single peak was fit; for the MRD500 spectra a sum of 2 of these functions was used.

The derived line shape function was fitted to the energy spectra using a non-linear algorithm known as the downhill simplex method [13]. This routine differs from relatively standard non-linear fitting techniques (such as the Levenberg-Marquardt method [14]) in that it requires only functional evaluations and not derivatives. This is convenient in some cases as the derivatives of the fitting function may be difficult to derive analytically. The results of the fitting procedure for the spectral data are shown in figures 7a and 7b as a solid line, for data obtained with both the MRD500 diode and the surface barrier detector. The reduced chi-square (χ^2_ν) for the fits to the spectral data were 1.19 (figure 7a) and 1.66 (figure 7b), indicating excellent agreement. The channel number corresponding to the mode (most probable value) of the line shape function, which was fit to the highest energy peak, was used to delineate the peak location, for a given transmitted ion energy.

The results of the analysis of the peak location for all the alpha energy spectra obtained with the MRD500 diode is shown in figure 8. The alpha energy was determined by TRIM simulation, as previously discussed. The average alpha particle energies ranged from 5.48 MeV (maximum vacuum attainable) to 0.85 MeV (57.2 cm Hg abs. air pressure). A weighted linear fit to the experimental data yielded a

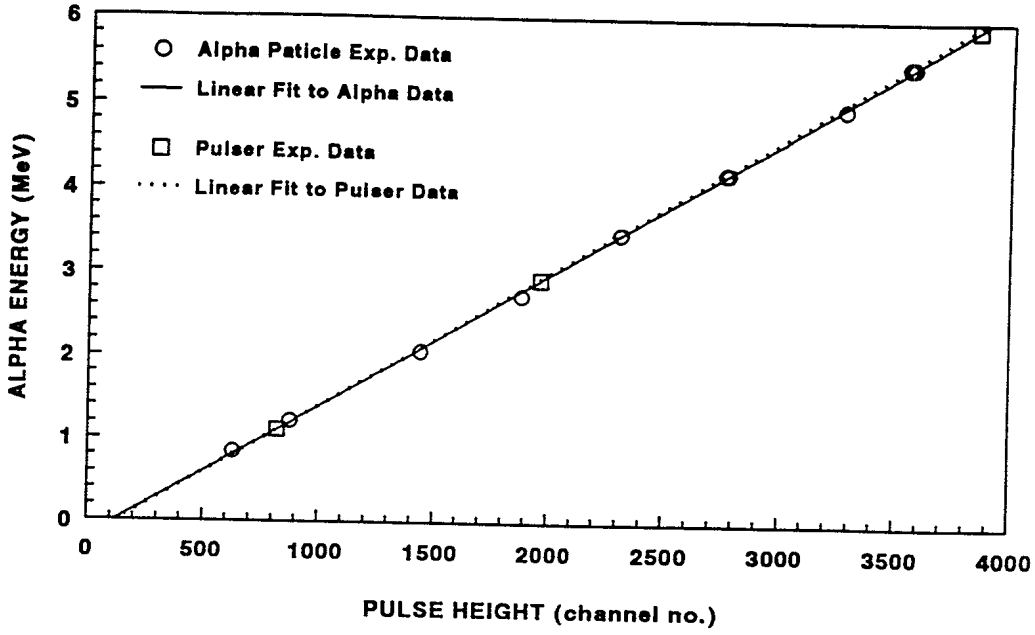

Figure 8. Experimental results for determination of alpha particle energy as a function charge collected, in terms of pulse height, from the MRD500 photodiode. The pulser reference data is also shown.

linear correlation coefficient r=0.9998, defined as [15]

$$r = \frac{N\sum x_i y_i - \sum x_i \sum y_i}{\sqrt{N\sum x_1^2 - \left(\sum x_i\right)^2}\sqrt{N\sum y_i^2 - \left(\sum y_i\right)^2}} \qquad (2)$$

The values of r range from 0, when there is no correlation, to ±1, then there is complete correlation. The above reported value of the linear correlation coefficient, therefore, indicates that the data is highly linearly correlated. The use of a linear correlation coefficient was adopted as a measure of the goodness of fit for linear functions, rather that the reduced chi-square (χ_ν^2), because of the difficulty in performing a mathematically rigorous error analysis. The estimation of errors, and as

subsequently follows, the presence of errors in the independent "x" values, renders the reduced chi-square unreliable as a goodness of fit indicator. The estimated errors associated with the experimental determination of the alpha particle energy (i.e. through TRIM simulations), although not indicated in figure 8, ranged from 0 percent at 5.48 MeV to approximately 10 percent at 0.85 MeV.

In figure 8, both the peak location and the alpha particle energy have errors associated with them, although the linear fit was performed with only a consideration of the error in the alpha energy. The channel number corresponding to mode of the main peak was treated as the independent variable, which usually doesn't have an error associated with it. This approach is justified since the percentage error in the peak location was much smaller than the percentage error in the transmitted alpha energy determination. For example, from the non-linear fit of the spectral shape, the error in the mode determination was estimated to be ±0.05% (i.e. ±2 channels) at 5.48 MeV and ±1.67% (i.e. ±10 channels) at 0.85 MeV. For the TRIM simulations performed, the reported error in the transmitted alpha energy reflects only the uncertainty due to experimentally measured parameters; the absolute accuracy of the value of the transmitted ion energy obtained from the TRIM simulations is not known and hence cannot be reported. This is due to the lack of published specific experimental data with which to compare the accuracy of the TRIM simulations. Reference [16] generally discusses the accuracy of the stopping powers generated by TRIM, but it is impossible to translate them into an error for the Monte Carlo ion transport simulation aspect of TRIM, unless detailed experimental data is available.

Also shown in figure 8 is a representative data set for the centroid locations for the Gaussian peaks obtained using the pulser reference signals. For a Gaussian distribution,

the mode and the centroid channels are identical. The relative magnitude of the amplitude of the pulser reference signals was 10:5:2, i.e. the centroids were located at channel numbers 3848.2±5.9, 1966.1±2.9 and 821.5±1.1, respectively. A linear fit to the pulser data (shown as a dotted line in figure 8) yielded a linear correlation coefficient of 0.9999. The numerical values for the slope were found to be $(1.59\pm0.01)\times10^{-3}$ Mev/channel for both fits. The y-intercepts were -0.1916±0.0239 MeV and -0.1950±.0010 MeV, for the alpha data and pulser data, respectively. The pulser and alpha particle data exhibit excellent agreement in both the y-intercept and slope (i.e. system conversion gain). This confirmation serves to validate the integrity of the TRIM-generated transmitted alpha particle energy data and the consistency in the data analysis technique for the estimation of the peak locations from the alpha spectra. Although not shown, the y-intercept was later subtracted from both the data and the best-fit line, in order to force the best-fit line to pass through the origin. The d.c. offset is an artifact of the pre-amplifier, amplifier and ADC instrumentation and, therefore, is legitimately subtracted.

The charge collection measurement data for laser-induced SEUs are shown in figure 9, where the absolute laser energy incident on the MRD500 die versus pulse height has been plotted. Each data point on the graph of figure 9, represents the pulse-height measured for a single laser shot. The error in the pulse-height data is mainly due to the SNR of the ADC's input signal and by the quantization error during signal digitization (±1/2 bit). The SNR is difficult to estimate with our experimental set-up, due to the uncontrolled fluctuation in experimental parameters on a shot-to-shot basis, however, we estimate that the error in the pulse-height, due to the above factors to be ±5 channels (approximately ±1.22% of full-scale). The error in the energy readings, as stated previously are estimated to be

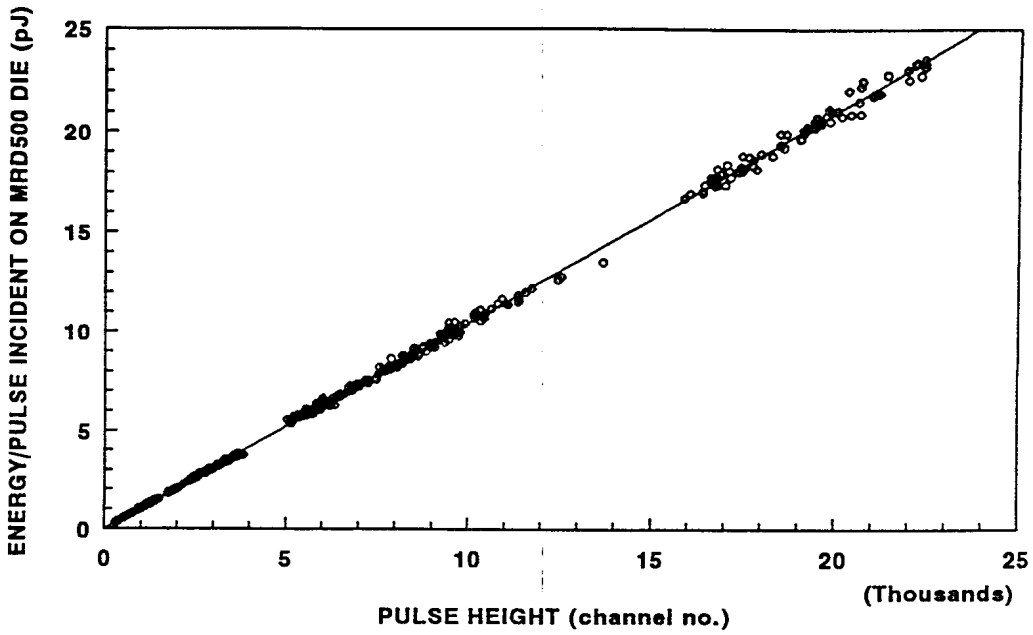

Figure 9. Experimental data for the measurement of laser pulse energy as a function of charge collected, in terms of pulse height, from the MRD500 photodiode.

±10%. The error bars are not shown in figure 9, due to the density of data points.

In figure 9, the pulse height data extends beyond the 4096 channel (i.e. 12 bit) digitization limit of the ADC. The input signal conversion limit (i.e. the effective number of bits of the ADC) was effectively extended, by decreasing the amplifier's gain, as the ADC's maximum input signal limit was reached. Through the analysis of the pulser data taken for the various amplifier gains used, the change in system gain could be measured accurately, thus correction factors could be applied to pulse height data obtained with the lower conversion gains. In figure 9, the data appears in three separate clusters, due to three separate gains used to during the experiment. The effective upper conversion limit was extended by a factor of about 5.6 using both the

coarse and fine gain adjustments available on the amplifier. The maximum pulse height attained in this work was for the lowest amplifier gain setting available.

The solid line in figure 9 is a linear fit of the laser pulse-energy versus channel number data. The linear correlation coefficient for the fit was 0.9997. The three sets of laser data which make up the graph presented in figure 9, had their respective y-intercepts, determined by a linear least-squares fit, subtracted before the data was combined. This was necessary because small differences were measured in the d.c. offsets as the amplifier gain was changed to obtain the three data sets. Both the data and the best-fit line shown in figure 9, therefore, reflect the fact that the y-intercept has been removed. The slope was determined to be $(1.059\pm0.001)\times10^{-15}$ J/channel. The residual y-intercept of the fit was $(-2.304\pm0.796)\times10^{-15}$ J.

The alpha particle pulse height data and the lower energy range of the laser pulse height data from figures 8 and 9 have been combined in figure 10, to give a linear calibration between laser energy and alpha particle energy that produce the same measured pulse height, for the MRD500 diode. Included in the graph is alpha particle data in the energy range of 0 to 5.48 MeV and laser pulse energies up to and including that which produce the same pulse height as a 5.48 MeV alpha particle. From a linear fit to the data, the linear correlation coefficient was 0.9994 and the slope 0.652 ± 0.008 pJ/MeV. The slope represents the calibration factor for the equivalence of laser pulse energy and alpha particle energy for creating electron-hole pairs in and near the depletion region. A fraction of the free carriers are subsequently collected and result in a measured pulse-height, which is proportional to the charge collected.

Figure 11 illustrates the calibration between laser

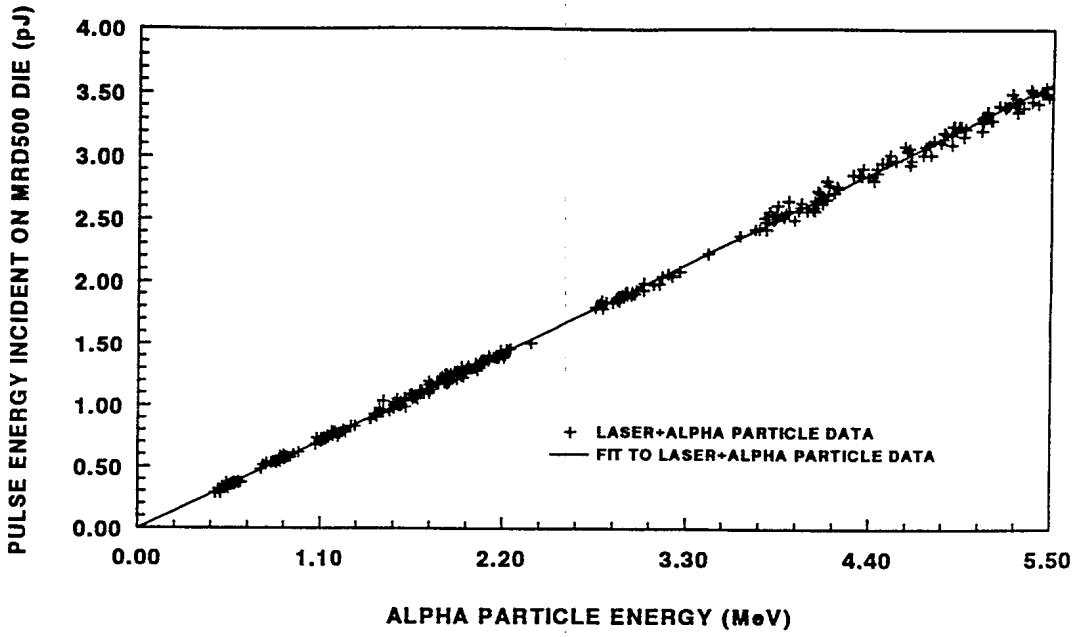

Figure 10. Experimental results for calibration for laser pulse energy and alpha particle energy that produce the same magnitude of collected charge in the MRD500 pin photodiode. The data shown is for alpha energies in the range of 0-5.48 MeV.

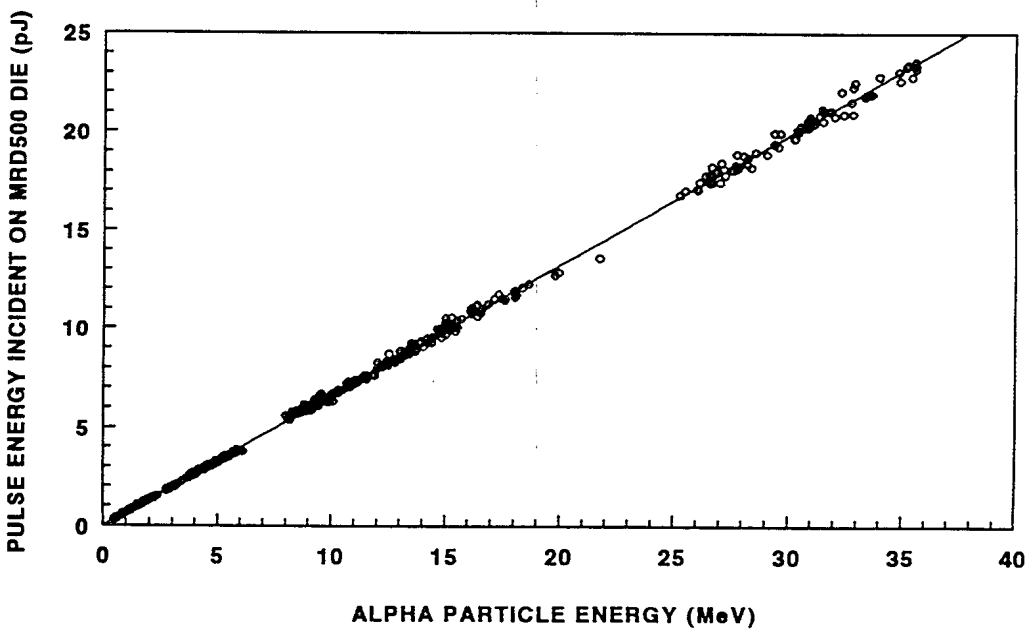

Figure 11. Extended calibration data for laser pulse energy and alpha particle energy that produce the same magnitude of collected charge in the MRD500 pin photodiode. The data points shown above 5.48 MeV equivalent alpha particle energy are for data obtained with the laser only.

energy and alpha energy for all the pulse-height data obtained. Obviously, all the data points above the equivalent of 5.48 MeV alpha energy are due to laser data only, since we were limited to a maximum alpha particle energy of 5.48 MeV. For the lowest gain available in the amplifier, the ADC saturated at a laser pulse energy of about 24 pJ, thereby limiting our measurements. From a linear least-squares fit to the data, the following parameters were calculated; slope=0.661±0.009 pJ/MeV, y-intercept=$(-2.31\pm0.80)\times10^{-2}$ pJ and r=0.9970. The slope obtained here agrees, within experimental error, with the value of 0.652±0.008 pJ/MeV reported for the data illustrated in figure 10. The latter value, however, was selected as the "calibration value", because it reflects the most accurate and precise data.

4.0 DISCUSSION

The experimental data has indicated that the laser can accurately simulate alpha particle-induced SEUs, in a MRD500 silicon pin photodiode, in the energy range between 0 and 5.48 MeV. With this alpha particle energy span, the corresponding linear energy transfer (LET) in silicon ranges from 0.585 MeV/(mg/cm^2) at 5.48 MeV to a maximum of 1.551 MeV/(mg/cm^2) at approximately 500 keV, as calculated by TRIM. Note that these LET values are valid at the surface of the device and not at the point of entering the depletion region. For the relatively low alpha energies used in this work, the range is relatively small and the energy loss and change in LET occur rapidly as a function of depth, compared with, say, a 40 MeV alpha particle. Above 5.48 MeV alpha particle energy, the laser has been shown capable of simulating up to the alpha particle energy equivalent of approximately a 36 MeV, assuming that the linear trend in pulse height response is valid for alpha particles above 5.48 MeV. If the laser pulse energy had

increased beyond our range of measurement capability, eventually the pulse height response would have become non-linear, possibly due to such factors as free carrier absorption effects [17]. For increasing alpha particle energies above 5.48 MeV, it is quite probable that the pulse height response to alpha particles would eventually become non-linear, but for a different reason. Ion range effects also have to be considered, as once the ion range becomes larger than the depletion width, the energy deposition will generally be non-linear with respect to ion energy. For example, a 5.5 MeV and a 40 MeV alpha particle have ranges in silicon of 27 μm and 701 μm, respectively. It is probable that the latter range exceeds the depletion depth of the device, so that a non-linear response might be expected.

The previous discussion can also explain why the calibration performed in this study is device specific. Two different devices with different thicknesses or types of surface passivation layers can cause a variation in the fraction of ion energy loss, for a given incident ion energy, that the ion experiences before it reaches the depletion region. This is further complicated by the possibility that the depletion regions of the two devices may have different thicknesses. This can also cause a variation of the energy deposited in the charge collection volume. These effects discussed above are minimized, however, for light and heavy ions of much higher energy, as the LET may vary only slightly as the ion travels from the surface of the device to the depletion region.

Similar variations can occur in different devices when they are exposed to pulsed 1060 nm radiation from the laser. Different materials (including the same material, but different doping densities) have different absorption coefficients, indexes of refraction and reflection/transmission coefficients. Optical properties

such as these can greatly affect the fraction of the incident laser energy reaching the depletion region. Again, varying depletion widths can also affect the fraction of laser energy absorbed.

From the calibration curve of laser pulse energy versus alpha particle energy, a value of 0.652±.008 pJ/MeV was obtained, which relates the amount of laser and alpha particle energy required to produce the same charge collection from the MRD500 diode. Since 1 MeV equals 1.60×10^{-13} J, or 0.160 pJ, it can be seen that approximately 4.08 times more incident laser energy is required than the energy of the alpha particle incident on the MRD500, to produce the same pulse height. One of the major factors accounting for this difference is the energy required to create an electron-hole pair in silicon. On average, an ion requires 3.6 eV to generate an electron-hole pair in silicon, while a 1.17 eV photon from the laser potentially can produce an electron hole pair. Some of the key factors contributing to the laser's charge-generation inefficiency are the absorptive and reflective losses at the surface, material interfaces and the bulk of the semiconductor device.

5.0 CONCLUSIONS

The Nd:Glass laser facility, developed in-house at Defence Research Establishment, has been described and the system's performance has been characterized in detail. A comparison of the charge collected from a silicon pin photodiode has been performed, due to alpha particle and ion-induced SEU in the device. A calibration has been obtained which gives the equivalence factor between alpha particle energy and laser pulse energy (at 1060 nm) in creating the same magnitude of SEU effect, namely the charge collected from the pin diode.

6.0 ACKNOWLEDGEMENTS

The authors wish to formally thank Mr. Joe Seregelyi, of the EMC/EMP group of EWD/CM, at DREO, for many helpful technical discussions regarding varied problems with pulsed lasers and methods of circumventing electrical noise problems due to pulsed lasers. With his kind advice and assistance, the design and construction of effective shielding enclosures for sensitive electronics was greatly accelerated.

7.0 REFERENCES

1. S. Buchner, K. Kang, W.J. Stapor, S. Rivet, IEEE Trans. Nucl. Sc., Vol 39, No. 6, pp 1630-1635, December 1992.

2. C. Gosset, B.W. Hughlock, A.H. Johnston, IEEE Trans. Nucl. Sc., Vol 39, No. 6, pp 1647-1653, December 1992.

3. D. McMorrow, J.S. Melinger, A.R. Knudson, A.B. Campbell, IEEE Trans. Nucl. Sc., Vol 39, No. 6, pp 1657-1664, December 1992.

4. R. Scheiderwind, D. Krening, S. Buchner, K. Kang, T. Weatherford, IEEE Trans. Nucl. Sc., Vol 39, No. 6, pp 1657-1664, December 1992.

5. D.H. Habing, IEEE Trans. on Nucl. Sci., Vol. NS-12, No. 5, p. 91, Oct. 1985.

6. "Motorola Optoelectronics Device Data", Motorola, Inc., U.S.A., 1989.

7. "Model 142IH Preamplifier Operating and Service Manual", EG&G Ortec, U.S.A.

8. "Table of Isotopes", Seventh Edition, C. Michael Lederer, Virginia S. Shirley eds., John Wiley & Sons, Inc., New York, 1978.

9. J.F. Ziegler, TRIM (Transport of Ions in Materials) Monte Carlo Computer Code, IBM Thomas Watson Research Center, Personal Communication.

10. G.T. Pepper, A. Fechete, "Observation of Optical Image Artifacts in a Linear Charge-Coupled Device", To be published as a Defence Research Establishment Ottawa Report.

11. "CRC Standard Mathematical Tables", S.M. Selby, ed., CRC Press, Inc., Cleveland Ohio, 1975.

12. "Handbook Of Mathematical Functions", M. Abramowitz, I.A. Stegun, eds., National Bureau of Standards, Applied Mathematics Series 55, United States Dept. of Commerce, Washington, 1968.

13. J.A. Nelder, R. Mead, Computer Journal, vol 7, p 308, 1965.

14. D.W. Marquardt, Soc. Ind. Appl. Math, 11, pp. 431-434, 1963.

15. P.R. Bevington, "Data Reduction and Analysis for the Physical Sciences", McGraw-Hill, Inc., New York, 1969.

16. J.F. Ziegler, J.P. Biersack, U. Littmark, "The Stopping and Range of Ions in Solids", Volume 1, Pergamon Press, New York, 1985.

17. A.K. Richter, I. Arimura, IEEE Trans. on Nucl. Sci., Vol. NS-34, No. 6, Dec. 1987.

UNCLASSIFIED

SECURITY CLASSIFICATION OF FORM
(highest classification of Title, Abstract, Keywords)

DOCUMENT CONTROL DATA

(Security classification of title, body of abstract and indexing annotation must be entered when the overall document is classified)

1. ORIGINATOR (the name and address of the organization preparing the document. Organizations for whom the document was prepared, e.g. Establishment sponsoring a contractor's report, or tasking agency, are entered in section 8.)

Defence Research Establishment Ottawa
Ottawa, Ontario
K1A 0Z4

2. SECURITY CLASSIFICATION (overall security classification of the document including special warning terms if applicable)

UNCLASSIFIED

3. TITLE (the complete document title as indicated on the title page. Its classification should be indicated by the appropriate abbreviation (S,C or U) in parentheses after the title.)

Characterization and Calibration of a Pulsed Laser System for Single Event Upset Simulation (U)

4. AUTHORS (Last name, first name, middle initial)

Pepper, G.T., Fechete, A.

5. DATE OF PUBLICATION (month and year of publication of document)

November 1994

6a. NO. OF PAGES (total containing information. Include Annexes, Appendices, etc.)

48

6b. NO. OF REFS (total cited in document)

17

7. DESCRIPTIVE NOTES (the category of the document, e.g. technical report, technical note or memorandum. If appropriate, enter the type of report, e.g. interim, progress, summary, annual or final. Give the inclusive dates when a specific reporting period is covered.

DREO Report

8. SPONSORING ACTIVITY (the name of the department project office or laboratory sponsoring the research and development. Include the address.

Defence Research Establishment Ottawa, 3701 Carling Avenue, Ottawa, K1A 0Z4

9a. PROJECT OR GRANT NO. (if appropriate, the applicable research and development project or grant number under which the document was written. Please specify whether project or grant)

Project 041LS

9b. CONTRACT NO. (if appropriate, the applicable number under which the document was written)

10a. ORIGINATOR'S DOCUMENT NUMBER (the official document number by which the document is identified by the originating activity. This number must be unique to this document.)

DREO REPORT 1241

10b. OTHER DOCUMENT NOS. (Any other numbers which may be assigned this document either by the originator or by the sponsor)

11. DOCUMENT AVAILABILITY (any limitations on further dissemination of the document, other than those imposed by security classification)

(X) Unlimited distribution
( ) Distribution limited to defence departments and defence contractors; further distribution only as approved
( ) Distribution limited to defence departments and Canadian defence contractors; further distribution only as approved
( ) Distribution limited to government departments and agencies; further distribution only as approved
( ) Distribution limited to defence departments; further distribution only as approved
( ) Other (please specify):

12. DOCUMENT ANNOUNCEMENT (any limitation to the bibliographic announcement of this document. This will normally correspond to the Document Availability (11). however, where further distribution (beyond the audience specified in 11) is possible, a wider announcement audience may be selected.)

Unlimited Announcement

UNCLASSIFIED

SECURITY CLASSIFICATION OF FORM

RA.W (21 Dec 92)

13. **ABSTRACT** (a brief and factual summary of the document. It may also appear elsewhere in the body of the document itself. It is highly desirable that the abstract of classified documents be unclassified. Each paragraph of the abstract shall begin with an indication of the security classification of the information in the paragraph (unless the document itself is unclassified) represented as (S), (C), or (U). It is not necessary to include here abstracts in both official languages unless the text is bilingual).

(U) A pulsed Nd:Glass laser facility that was developed at Defence Research Establishment Ottawa, for the simulation of single event upsets (SEUs) in electronics, is described in detail. The performance of the laser system, the associated instrumentation and data acquisition systems were extensively characterized during the process of studying the charge collected in a silicon p-i-n photodiode, due to laser and ion-induced SEU. Laser simulation of SEUs is demonstrated to be an accurate and convenient complementary method to ion accelerator-based SEU experimentation.

14. **KEYWORDS, DESCRIPTORS or IDENTIFIERS** (technically meaningful terms or short phrases that characterize a document and could be helpful in cataloguing the document. They should be selected so that no security classification is required. Identifiers, such as equipment model designation, trade name, military project code name, geographic location may also be included. If possible keywords should be selected from a published thesaurus, e.g. Thesaurus of Engineering and Scientific Terms (TEST) and that thesaurus-identified. If it is not possible to select indexing terms which are Unclassified, the classification of each should be indicated as with the title.)

single event upset
SEU
radiation effects on electronics
pulsed laser system
single event upset simulation
laser-induced single event upset
laser-induced SEU